Control of SiC Based Integrated DC-DC Powertrain Charger for Electric Vehicles

Saeed Anwar and Daniel Costinett
Department of Electrical Engineering and Computer Science
The University of Tennessee, Knoxville
Knoxville, TN, USA
sanwar@vols.utk.edu

Subhajyoti Mukherjee and Shajjad Chowdhury
Power Electronics and Electrical Machinery Group
Oak Ridge National Laboratory
Oak Ridge, TN, USA

***Abstract*— In this paper, an automated controller for an integrated, reconfigurable dc-dc converter for plugin electric vehicles (EVs) is presented. The integrated converter combines both an interleaved boost converter and dual active bridge (DAB) converter, sharing magnetics and switching devices. The converter switches between operating modes using the existing battery management system (BMS) contactors. The integrated converter operates in isolated DAB mode during battery charging operation. During traction operation, the integrated converter is operated in interleaved boost mode for heavy load and DAB mode during light load, high voltage operation. An online transition algorithm is used to transition from interleaved boost mode to DAB mode with minimal bus distortion. The automated controller selects the operating mode and inverter bus voltage at different torque-speed conditions to get maximum overall traction drive efficiency. An experimental prototype of the integrated converter demonstrates the automated controller functionality.**

Keywords*— integrated converter, online mode transition, hybrid transformer, closed loop control, dual active bridge converter, interleaved boost converter.

I. Introduction

The design challenges for the next generation EV power converters are efficiency improvement, reduced weight and volume of passive elements, compact size, and overall cost reduction. An integrated converter can reduce the converter weight, size, and cost by sharing magnetics, power switches, and capacitors [1-4]. However, integrated converters often reduce the efficiency of the overall system by reusing power switches or passive elements [5].

The integrated dc-dc converter topology presented in [1] combines the isolated dc-dc stage of an on-board charger and drivetrain interleaved boost converter as shown in Fig. 1. Using the BMS contactors, the converter can be reconfigured in both DAB mode and interleaved boost mode. By operating in DAB mode, the integrated dc-dc converter has improved efficiency at light load and high-voltage compared to a separate boost converter. This work focuses on the control design for the integrated topology.

Control of integrated converter requires accommodating operation in different modes and managing transitions between them during online reconfiguration. Different closed-loop voltage controllers are studied in [6, 7] for the boost converter. In the integrated dc-dc converter, the magnetizing inductance of the transformer is used as the boost inductor. As a result, the magnitudes of the magnetizing and leakage inductances are

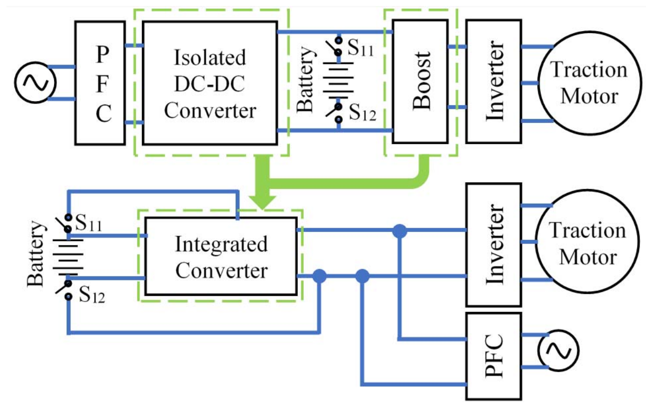

Fig. 1. Integrated powertrain-charger architecture for EVs [1].

comparable. Different modeling and control approaches are also investigated for DAB converters [8-10]. To evaluate the plant model for DAB mode, the magnetizing current needs to be modeled. Fast dynamic control is required during mode transitions to prevent extended transients during reconfiguration, while ensuring zero-voltage turn-on and zero-current turn-off of the BMS contactors.

In this paper, a closed-loop control strategy is presented for the integrated dc-dc converter. The primary role of the controller is to regulate the voltage of the integrated converter. In interleaved boost configuration, the controller is also responsible for current balancing between the interleaved phases; in DAB mode the controller must eliminate dc offset to prevent the transformer saturation.

The paper is organized as follows. The integrated converter operating modes are presented in Section II. The automated controller control methodology is presented in Section III. The experimental prototype and testing results are presented in Section IV. Conclusions and future works are stated in Section V.

II. Integrated Converter Operating Modes

The integrated topology design and steady-state analysis are presented in [1]. The circuit diagram of the integrated converter topology in interleaved boost mode is shown in Fig. 2. The secondary side self-inductance is used for boost inductor. The switches in the primary H-bridge (S_1-S_4) are turned-off during interleaved boost operation. The switches in the secondary H-

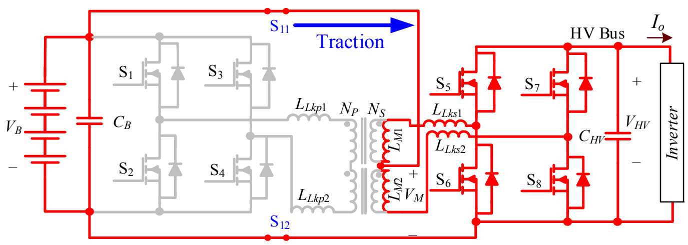

Fig. 2. Integrated converter in interleaved boost mode.

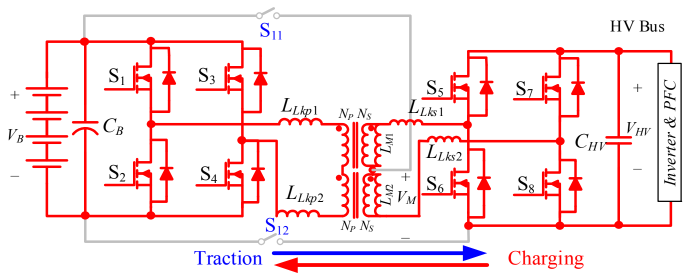

Fig. 3. Integrated converter in DAB mode.

bridge (S_5-S_8) are operated to boost the battery voltage for the traction inverter,

$$V_{HV} = \frac{1}{1-D} V_B \tag{1}$$

where D and V_B are the converter duty ratio and battery voltage, respectively. The bidirectional boost converter steps up the battery voltage to allow the inverter to operate at higher efficiency based on different loads. The boost stage decouples the inverter operation and regulates the voltage regardless of the varying state of the charge (SOC) of the battery. The boost mode of the integrated converter is rated for full traction power.

The circuit diagram of the integrated converter topology in DAB mode is shown in Fig. 3. The DAB is capable of bidirectional power flow, and thus can be used in both in both traction and battery charging operation. The DAB converter is rated for Level II charging. The power flow of the integrated converter [11] in DAB mode is

$$P_{DAB} = \frac{n_{eff} V_B V_{HV} \phi(\pi - |\phi|)}{2 f_{sDAB} L_{eq}} \tag{2}$$

where n_{eff}, V_B, V_{HV}, ϕ, f_{sDAB}, and L_{eq} are the transformer effective turns ratio, battery voltage, inverter bus voltage, phase shift, DAB switching frequency, and equivalent leakage inductance of the hybrid transformer, respectively. The equivalent leakage inductance [11] is

$$L_{eq} = \left(n_{eff}^2 L_{Lkp} + L_{Lks} + \frac{n_{eff}^2 L_{Lkp} L_{Lks}}{L_M} \right) \tag{3}$$

where L_{Lkp}, L_{Lks}, and L_M are the primary leakage inductance, secondary leakage inductance, and magnetizing inductance. During light-load, high-voltage traction operation, the interleaved boost mode efficiency is low. So, the integrated converter is reconfigured in DAB mode to improve traction efficiency.

An open-loop transition algorithm between the interleaved boost and DAB mode is presented in [12] to ensure smooth transition between modes and stable inverter bus voltage during the mode transition. The reconfiguration between boost and DAB mode is achieved by controlling the BMS contactor switches S_{11} and S_{12}. The contactors are closed when the midpoint voltage (V_M) is same as battery voltage to prevent inrush current. The winding currents are also set to zero before disconnecting S_{11} to prevent arcing.

III. Control Methodology

The controller adjusts the operating mode and output voltage of the integrated converter to maximize efficiency at each operating point. A lookup table based on analytical modeling in [11] is used to determine the operating mode and output voltage reference based on the sensed output power. When a mode transition occurs, the mode transition controller executes a fixed switching pattern based on the approach in [12] to transition between modes while minimizing contactor stresses during reconfiguration.

In DAB mode, the converter operates as a phase-shift modulated DAB. Including the impact of the magnetizing inductance, the control-to-output voltage transfer function [13] in phase shift DAB mode is

$$G_{v\phi}(s) = \frac{n_{eff} V_B \left(1 - \frac{2\phi}{\pi}\right) R_{load}}{(C_{HV} R_{load} s + 1) L_{eq}} \tag{4}$$

where, R_{load} and C_{HV} are the equivalent output load resistance and high-voltage bus capacitance.

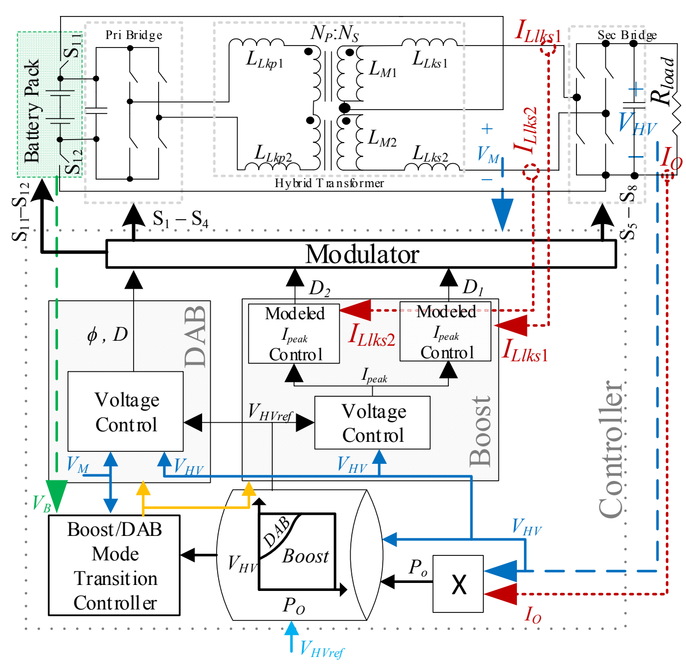

Fig. 4. Control architecture of the integrated converter.

The DAB is controlled by a proportional-integral (PI) controller, shown in Fig. 4, to set the phase shift of the controller based on the HV inverter bus voltage reference. The compensator is designed to achieve 1 kHz bandwidth for 220 V battery voltage and 600 V output voltage at 6.6 kW phase shift DAB operation. The phase margin is kept above 60□ for stable operation. The converter stability is also ensured for lower voltage level and lighter load conditions. As a result, the compensator provides fast transient for load step change and output load variation while ensuring the stability of the converter in DAB mode. The loop gain for the integrated converter in DAB mode is given in Fig. 5.

In the interleaved boost mode, the converter current is actively controller to ensure equal current between the phases. In interleaved boost mode, the boost converter transfer function is

$$G_{v_{HV}d} = \frac{\frac{V_B}{(1-D)^2}\left(1 - \frac{sL_{bx}}{R_{Load}(1-D)^2}\right)}{1 + \frac{sL_{bx}}{R_{Load}(1-D)^2} + \frac{L_{bx}C_{HV}(R_{Load})s^2}{R_{Load}(1-D)^2}} \qquad (5)$$

where D and L_{bx} are the boost converter duty cycle and secondary side self-inductance. The secondary side self-inductance including the secondary side leakage and magnetizing inductance of the hybrid transformer.

In the interleaved boost mode, shown in Fig. 4, a separate PI controller is used to generate the reference current i_{peak}. The average current of both boost inductors are sensed in each switching period. The peak inductor current is estimated according to [7, 14] as

$$i_{Llkx_{peak}}[n-1] = i_{Llkx_{av}} + \frac{V_B d[n-1]}{2 f_{sw_b} L_{bx}} \qquad (6)$$

where x, i_{Llkxav}, f_{swb}, $d[n-1]$, and L_{bx} are the phase number, average inductor current, switching frequency of boost converter, previous period duty cycle, and boost inductance, respectively. The duty cycle

$$d[n] = \frac{\frac{i_c}{2} - i_{Llkx_{peak}}[n-1]}{m_c} f_{sw_b} \qquad (7)$$

is calculated for each phase using the estimated peak current controller presented in [7, 14]. where m_c is the slope compensation which is set to

$$m_c = \frac{V_{HV} - V_B}{L_{bx}} \qquad (8)$$

The compensator is designed to achieve 1 kHz bandwidth for 220 V battery voltage and 600 V output voltage at 20 kW interleaved boost operation. The phase margin is kept above 60□ for stable operation. As a result, the compensator provides fast transient response based on the reference voltage change and output load variation. The loop gain of the integrated converter in boost mode is shown in Fig. 6.

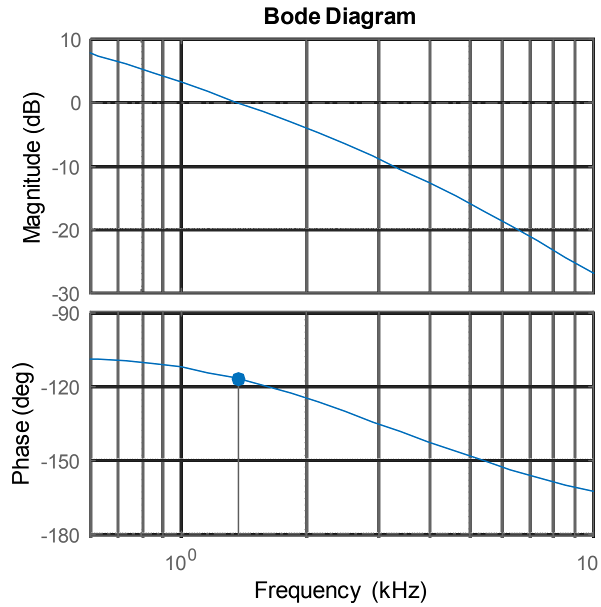

Fig. 5. Loop gain of the integrated converter in DAB mode.

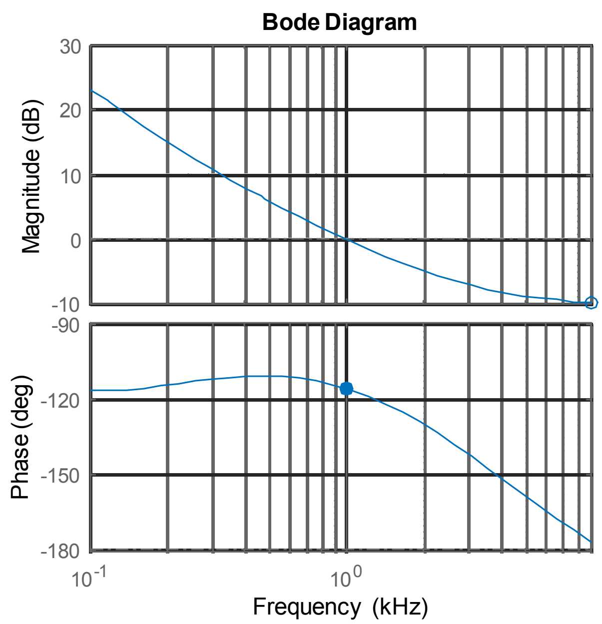

Fig. 6. Loop gain of the integrated converter in boost mode.

During the traction operation, the output power is monitored by the proposed controller. The inverter bus voltage is regulated to achieve maximum overall traction efficiecny at different power level which includes the integrated DC-DC converter, inverter, and motor efficiecny. A lookup table is generated with maximum efficiency and recommended inverter bus voltage level at different torque-speed condition or output power condition. The controller will automatically set the output voltage reference to achieve best overall traction efficiecny. The converter will automatically initiate online transition of the integrated DC-DC converter between the interleaved boost mode and DAB mode based on the output power level to improve efficiency further. The online transition between the interleaved boost and DAB mode presented in [12] is also regulated using the closed loop controllers. Trapezoidal DAB modulation is used by the transition controller, shown in Fig. 4, to ensure zero voltage across the BMS contactor. While closing the BMS contactor, voltage mismatch across the contactor triggers large inrush current and can damage the contactor. While opening the BMS contactor, flowing current can cause arcing and damage the contactor. To prevent damaging the BMS contactor, the midpoint voltage (V_M) of the hybrid transformer is regulated by the proposed controller during the transition. The DAB converter duty is modulated according to the method described in [12] to ensure the midpoint voltage (V_M) of the hybrid transformer is the same as the battery voltage.

IV. Experimental Results

An integrated converter prototype, fabricated at the National Transportation Research Center at Oak Ridge National Lab as shown in Fig. 7, is used to validate converter operation. The prototype integrates a two-phase, 20kW interleaved boost converter and a 6.6 kW DAB. Two parallel CREE C3M0030090K discrete SiC devices are used for each switch (S_1-S_4) in the primary side H-bridge. A custom SiC power module fabricated at ORNL [15, 16] is used as the secondary side H-bridge. The hybrid transformer is shown in Fig. 8 and its parameters are given in Table 1.

The integrated converter is controlled with TI F28335 DSP. Each phase of the interleaved boost currents is sensed using an LA 100 P current sensor with 200 kHz bandwidth. The output current is sensed using an LF 205-S sensor with 100 kHz bandwidth. The midpoint voltage and output voltage are sensed with LV25 P and CV 3 1000 sensors, respectively.

The interleaved boost converter is tested up to 20 kW for 400 V to 600 V output voltage. The efficiency comparison of the integrated converter operating at boost mode and DAB mode at 600V output voltage is shown in Fig. 9. The DAB mode exhibits superior efficiency for power levels below 6 kW.

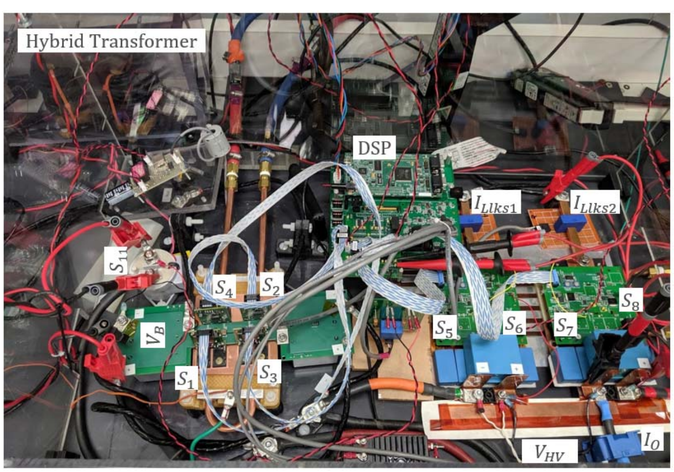

Fig. 7. Experimental prototype for 20 kW system.

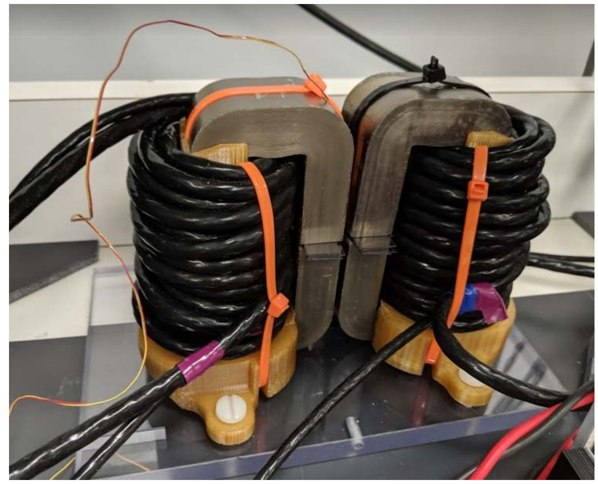

Fig. 8. Hybrid transformer for the integrated converter.

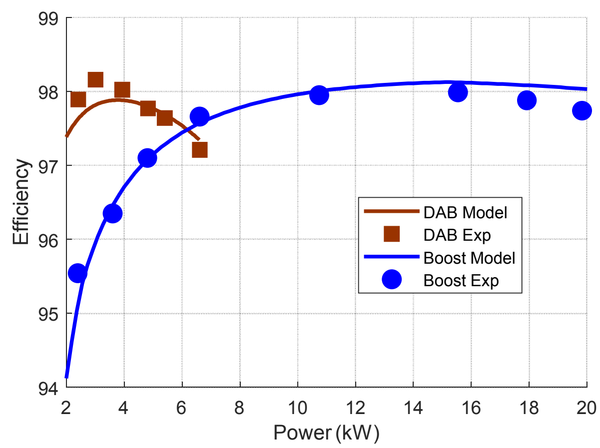

Fig. 9. Integrated converter efficiency comparison between boost mode and DAB mode.

In boost mode, the converter is operated at 50 kHz switching frequency. The waveforms for the interleaved boost mode without current control are shown in Fig. 10(a). The current is imbalanced between the phases due to imperfect matching between the two boost inductors. Using the current programmed control, the current is balanced evenly between the two interleaved boost windings as shown in Fig. 10(b). To visualize the dynamics of the interleaved boost converter control system, the output voltage reference is changed from 100 V to 108 V as shown in Fig. 11. The boost converter adjusts the output voltage according to the reference voltage step change within 1 ms. The phase currents are also distributed evenly during the transition.

In DAB mode, the converter is switched at 60 kHz. An open-loop phase-shift step response of the DAB is shown in Fig. 12 for operation at 2 kW. The transient time is over 12 ms. Using the closed loop DAB controller designed in the previous section, the response time is reduced to 0.5 ms with a step change in voltage reference from 400 V to 405 V as shown in Fig. 13.

The closed-loop output voltage step responses are compared to the small signal models in Fig. 11 for boost mode and Fig. 13 for DAB mode, showing good agreement.

TABLE I

INTEGRATED CONVERTER PARAMETERS

Parameters	Value / Type	Part No.
Primary device	Two parallel discrete SiC MOSFETs	C3M0030090K
Secondary device	Custom power module	[15, 16]
Hybrid Core	Nanocrystalline core	F3CC0125
Primary turns	9	
Secondary turns	26	
Primary self-inductance	33.87 µH	
Secondary self-inductance	238.5 µH	
Boost switching frequency	50 kHz	
DAB switching frequency	60 kHz	
Output capacitance	150 µF	

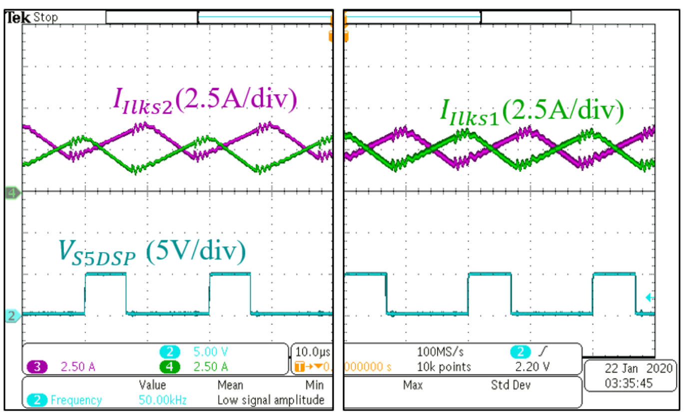

(a) (b)

Fig. 10. Interleaved boost mode of operation (a) without current control (b) with current control.

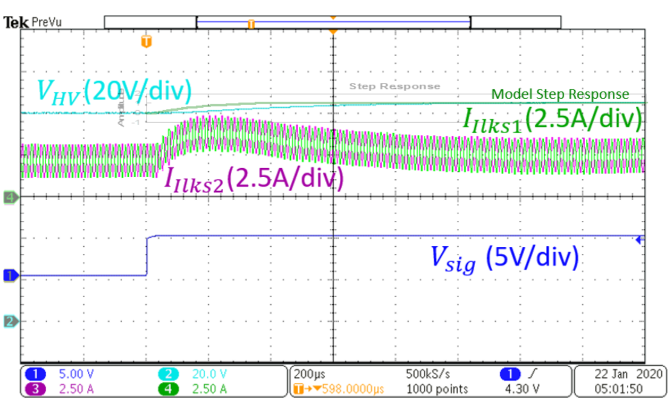

Fig. 11. Voltage step change using closed loop control of interleaved boost converter.

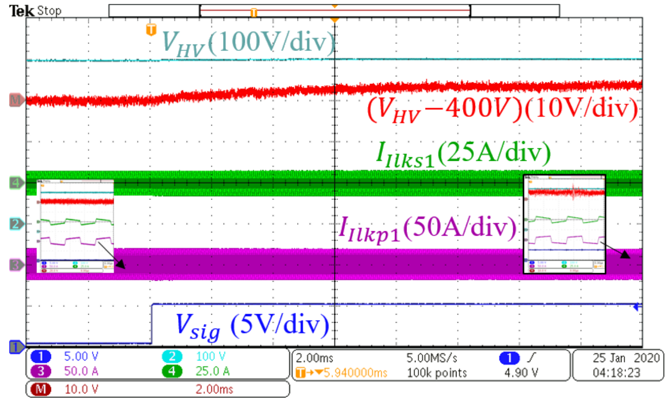

Fig. 12. Open-loop phase-shift step response of the DAB.

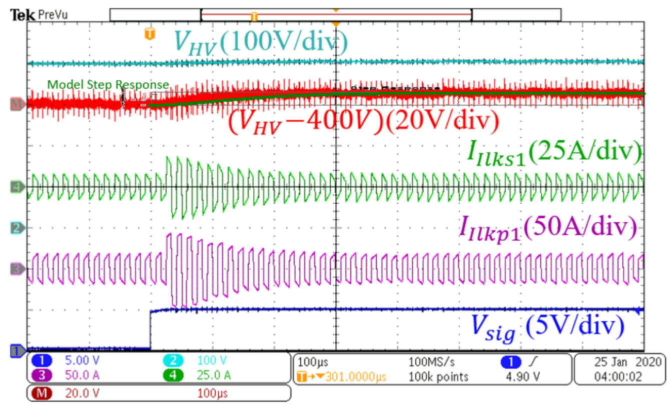

Fig. 13. Voltage step change using closed loop DAB controller.

Using an online transition algorithm [12] during traction operation, the converter switches to DAB mode to improve light load efficiency. The online transition from boost to DAB mode at 3 kW at 600 V bus voltage is shown in Fig. 14. The boost to DAB transition time is estimated at around 8.4 ms. At the onset of the boost to DAB transition, the interleaved boost currents are reduced to zero as shown in Fig. 15. After four switching cycles, the DAB mode is initiated using trapezoidal modulation. The duty cycle of the trapezoidal modulation is regulated by the controller to ensure zero voltage across the BMS contactor S_{11}. The startup process of the DAB mode is performed without any voltage or current oscillation. The BMS contractor is disconnected during the trapezoidal modulation since the current is diverted from the BMS contractor to the hybrid transformer. The transition from trapezoidal modulation to phase-shift modulation is performed after 8.4 ms as shown in Fig. 16. The phase shift modulation provides lower loss since the current peaks are reduced. Because power flow is continuous during the transition, V_{HV} remains stable during the entire mode transition.

Once the integrated converter power demand exceeds 6.6 kW, the converter makes the transition from DAB mode to boost mode. The online transition from DAB to Boost mode at 7 kW is presented in Fig. 17. The total transition time is around 20 ms. At the onset of the transition, the BMS contactor signal is turned on and the DAB modulation is changed from phase shift modulation to trapezoidal modulation as shown in Fig. 18. The duty cycle of the trapezoidal modulation is controlled by the controller to ensure the voltage across the BMS contactor S_{11}. After the BMS contactor connection time and bouncing time, the transition from DAB to boost mode is performed as shown in Fig. 19. The inductor current is ramped up to the modeled peak steady-state boost current to charge the output capacitor and reduce the current oscillation.

During the drive cycle, the integrated converter power demand varies for different torque and speed requirements. The operation of the integrated converter in a drive cycle is presented in Fig. 20. The converter is started using a soft start of the output voltage controller and constant current load. The output load is then programmed to change after 30 seconds to emulate the varying demand of the electric drive during a realistic drive cycle scenario. The closed loop controller ensures stable operation at different operating modes for different output voltage and power level.

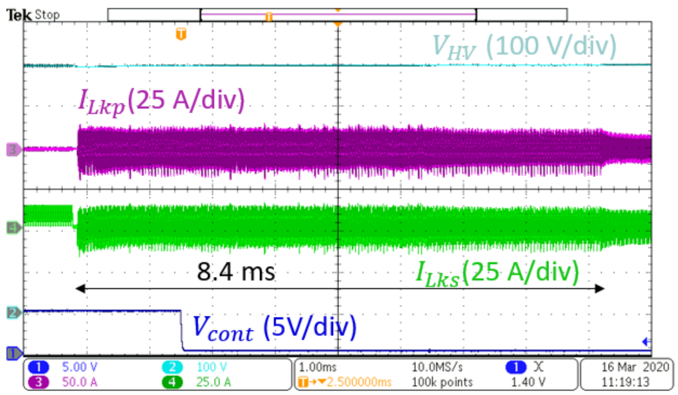

Fig. 14. Boost mode to DAB mode transition at 3 kW.

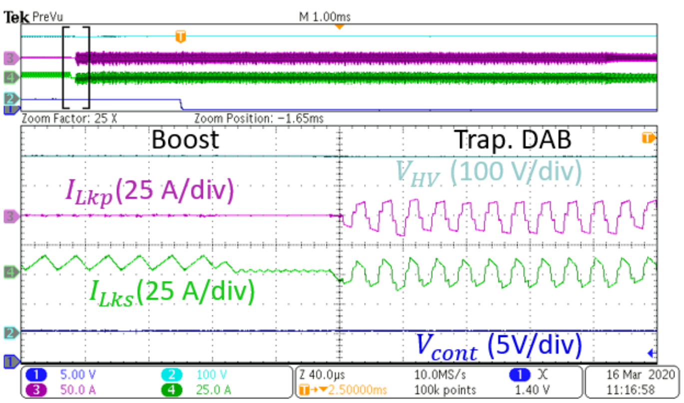

Fig. 15. Boost to Trapezoidal DAB transition at 3 kW.

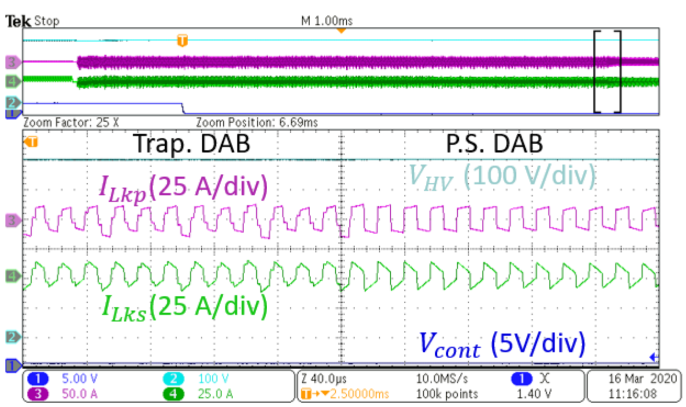

Fig. 16. Trapezoidal DAB to phase shift DAB transition at 3 kW.

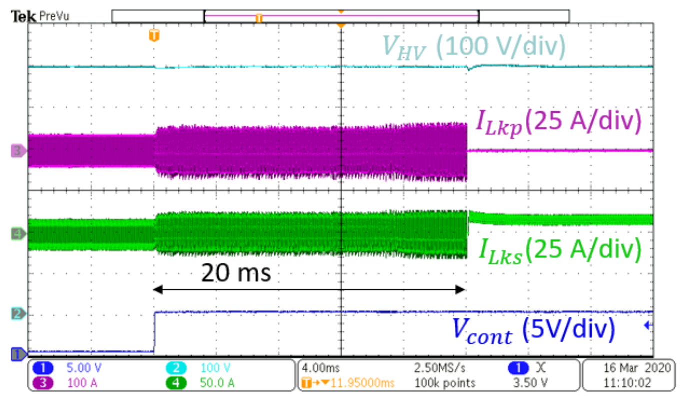

Fig. 17. DAB to interleaved Boost mode transition at 7 kW.

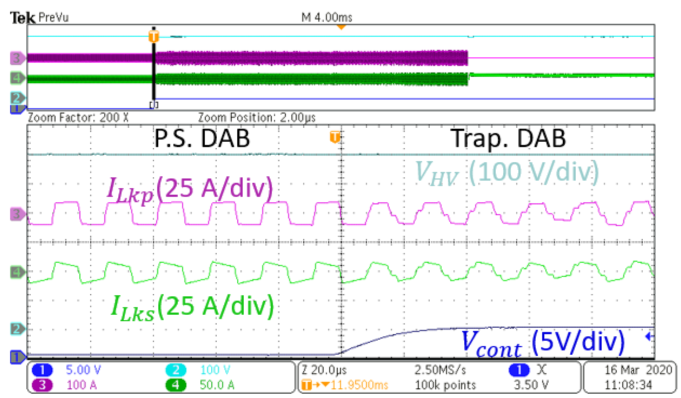

Fig. 18. Phase shift to trapezoidal DAB at 7 kW.

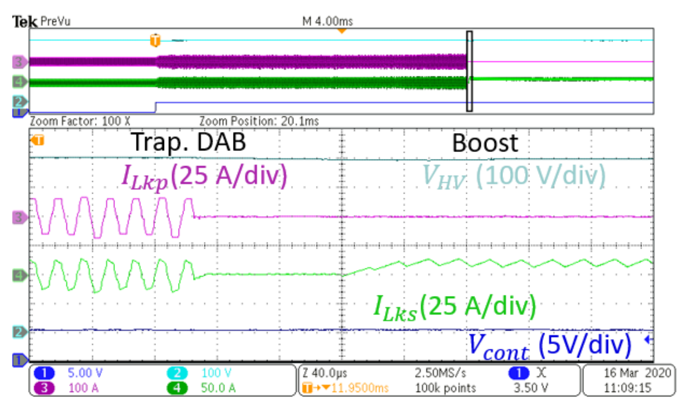

Fig. 19. Trapezoidal DAB to Boost transition at 7 kW.

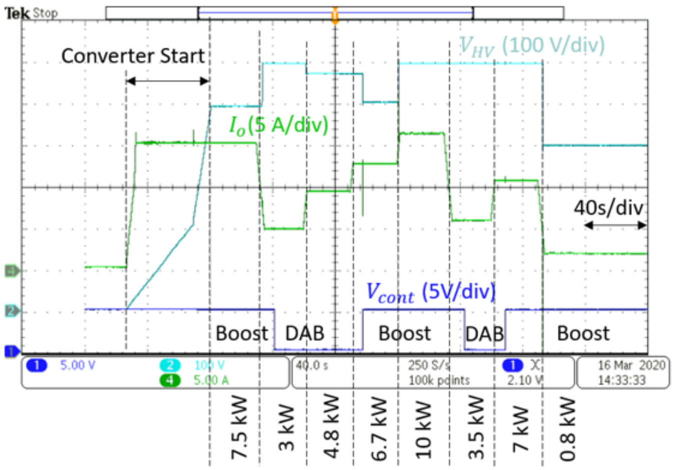

Fig. 20. Integrated converter operation during the drive cycle.

Based on the sensed output power, the converter automatically selects the operating mode and output voltage reference in order to maximize system efficiency from battery to mechanical power. A look-up table is stored on the DSP which contains the most efficient operating voltage and mode for any torque-speed combination, based on analytical modeling of the converter and measurements of the motor and drive. When a mode transition occurs, the online mode transition controller follows the switching patterns outlined previously to allow smooth transition between modes without power flow interruption. As a result, the overall traction loss is reduced over a drive cycle by automatic adjustment of the integrated dc-dc converter operating mode and output voltage.

V. Conclusion

This paper presents a closed loop automated control architecture for an integrated dc-dc converter for plugin EVs. The closed-loop controller is essential to regulate the output voltage and converter current for varying operating conditions during the drive cycle. During interleaved boost mode, the controller is responsible for current balancing between the interleaved phases. The converter control-to-output behavior in each mode is presented, and a controller is developed which operates in both modes and during transitions between them. The controller performance is demonstrated using a 20 kW SiC-based integrated converter prototype. The online transition between the boost and DAB is presented at different power level during the traction operation of the integrated converter operation. The traction boost converter efficiency drops at light load high voltage traction operation. The light load traction efficiency is improved by the automated online transition from interleaved boost mode to DAB mode. In this way, overall traction loss in a drive cycle is reduced and higher driving range can be achieved.

Acknowledgment

This work made use of the Engineering Research Center Shared Facilities supported by the Engineering Research Center Program of the National Science Foundation and DOE under NSF Award Number EEC-1041877 and the CURENT Industry Partnership Program.

This work used equipment and facilities at Oak Ridge National Laboratory. The authors like to acknowledge ORNL researchers including Dr. Omer Onar and Dr. Veda Galigekere for research guidance throughout the project, Dr. Emre Gurpinar for gate driver and thermal design, Jon Wilkins for hardware development and integrated magnetics prototyping, Steven Campbell for testing assistance, Larry Seiber for hardware development, and Cliff White for design of the digital control platform.

The SiC gate driver used in this work was previously built and validated under the DOE VTO project, "Highly Integrated Power Module." The authors also gratefully acknowledge the DOE VTO program for funding.

References

[1] S. Anwar, W. M. Zhang, F. Wang, and D. J. Costinett, "Integrated DC-DC Converter Design for Electric Vehicle Powertrains," *IEEE Applied Power Electronics Conference and Exposition,* pp. 424-431, 2016.

[2] K. Itoh, M. Ishigaki, N. Yanagizawa, S. Tomura, and T. Umeno, "Analysis and Design of a Multiport Converter Using a Magnetic Coupling Inductor Technique," *IEEE Transactions on Industry Applications,* vol. 51, no. 2, pp. 1713-1721, 2015.

[3] M. Chinthavali, O. C. Onar, S. L. Campbell, and L. M. Tolbert, "All-SiC inductively coupled charger with integrated plug-in and boost functionalities for PEV applications," in *2016 IEEE Applied Power Electronics Conference and Exposition (APEC)*, 20-24 March 2016 2016, pp. 1307-1314.

[4] S. Dusmez and A. Khaligh, "A Compact and Integrated Multifunctional Power Electronic Interface for Plug-in Electric Vehicles," *IEEE Transactions on Power Electronics,* vol. 28, no. 12, pp. 5690-5701, 2013.

[5] Y. Lee, A. Khaligh, and A. Emadi, "Advanced Integrated Bidirectional AC/DC and DC/DC Converter for Plug-In Hybrid Electric Vehicles," *IEEE Transactions on Vehicular Technology,* vol. 58, no. 8, pp. 3970-3980, 2009.

[6] Y. Huangfu, S. Zhuo, F. Chen, S. Pang, D. Zhao, and F. Gao, "Robust Voltage Control of Floating Interleaved Boost Converter for Fuel Cell Systems," *IEEE Transactions on Industry Applications,* vol. 54, no. 1, pp. 665-674, 2018.

[7] C. Jingquan, A. Prodic, R. W. Erickson, and D. Maksimovic, "Predictive digital current programmed control," *IEEE Transactions on Power Electronics,* vol. 18, no. 1, pp. 411-419, 2003.

[8] A. Kumar, A. H. Bhat, and P. Agarwal, "Review and comparative analysis of dual active bridge isolated DC to DC converter with different control techniques," *International Journal of Industrial Electronics and Drives,* vol. 4, no. 2, pp. 69-84, 2018.

[9] F. Krismer and J. W. Kolar, "Accurate Small-Signal Model for the Digital Control of an Automotive Bidirectional Dual Active Bridge," *IEEE Transactions on Power Electronics,* vol. 24, no. 12, pp. 2756-2768, 2009.

[10] H. Qin and J. W. Kimball, "Closed-Loop Control of DC–DC Dual-Active-Bridge Converters Driving Single-Phase Inverters," *IEEE Transactions on Power Electronics,* vol. 29, no. 2, pp. 1006-1017, 2014.

[11] S. Anwar and D. Costinett, "Modeling Dual Active Bridge Converter Considering the Effect of Magnetizing Inductance for Electric Vehicle Application," in *2018 IEEE Energy Conversion Congress and Exposition (ECCE)*, 23-27 Sept. 2018 2018, pp. 538-545.

[12] S. Anwar and D. J. Costinett, "Operating mode transition control of a SiC integrated DC DC powertrain charger for electric vehicles," in *IEEE Transportation Electrification Conference and Expo*, 2017, pp. 152-157.

[13] D. Costinett, R. Zane, and D. Maksimovic, "Discrete time modeling of output disturbances in the dual active bridge converter," in *2014 IEEE Applied Power Electronics Conference and Exposition - APEC 2014*, 16-20 March 2014 2014, pp. 1171-1177.

[14] S. Chattopadhyay and S. Das, "A Digital Current-Mode Control Technique for DC–DC Converters," *IEEE Transactions on Power Electronics,* vol. 21, no. 6, pp. 1718-1726, 2006.

[15] Z. Wang, F. Yang, S. L. Campbell, and M. Chinthavali, "Characterization of SiC Trench MOSFETs in a Low-Inductance Power Module Package," *IEEE Transactions on Industry Applications,* vol. 55, no. 4, pp. 4157-4166, 2019.

[16] Z. J. Wang, F. Yang, S. Campbell, and M. Chinthavali, "Development of a low-inductance SiC trench MOSFET power module for high-frequency application," in *2018 IEEE Applied Power Electronics Conference and Exposition (APEC)*, 4-8 March 2018 2018, pp. 2834-2841.